

## ORIGINAL ARTICLE

# Effects of hairline cracks on the fracture behavior of polyethylene terephthalate injection moldings

Bernard Chukwuemeka Ogazi-Onyemaechi, Yew Wei Leong and Hiroyuki Hamada

Hairline cracks are microscopic defects found in most injection-molded components. The effects of such hairline cracks on the fracture modes of injection moldings, especially polyethylene terephthalate (PET), are still not well understood. The slow crystallizing nature of PET results in a distinct skin-core structure when it is injection molded. By controlling the hairline crack depth, the crack tip can be situated within the skin region of the moldings. The fracture behavior of hairline-cracked PET specimens during tensile loading was found to be dependent not only on the crack depth but also on the region in which the crack tips were situated. In contrast to our previous studies on a standard v-notch, very shallow hairline cracks resulted in catastrophic fracture of PET components. Crystallinity distribution along the skin core was found to affect the notch sensitivity of the materials. Annealing the specimens in hot oil was expected to create a crystallized outermost skin (referred to as the pseudo-skin) in the samples and remove internal stresses. This was intended to alter the skin-core ratio to evaluate its effect on the toughness of hairline-cracked specimens. The results revealed that annealing created a pseudo-skin layer and improved the toughness of the materials.

*Polymer Journal* (2010) 42, 887–895; doi:10.1038/pj.2010.86; published online 15 September 2010

**Keywords:** annealing; hairline crack; stress concentrators; notch sensitivity factor for energy; notch sensitivity factor for strength; toughness

## INTRODUCTION

Very sharp microscopic defects are known to affect the fracture modes of engineering components. Unlike v-notches,<sup>1</sup> crack initiation and propagation in sharp microscopic cracks (also known as hairline cracks) is very rapid and catastrophic. It is believed that a shallow hairline crack can cause a drastic change in the fracture behavior of polyethylene terephthalate (PET) injection moldings. The skin-core structure of injection moldings is believed to affect their fracture modes. Another element of interest in the fracture modes of hairline-cracked injection-molded PET components is the possible effect of annealing. It is believed that annealing the components in hot oil creates a crystallized outermost skin (referred to as the pseudo-skin). Annealing is performed uniformly to remove internal stresses, thus improving the fracture toughness of the materials. A study revealed that the differences in the percent crystallinity and residual stress levels between the skin and core layers decreased considerably after annealing.<sup>2</sup> However, in another study, injection-molded PET was annealed at 120 °C for 4 h to increase its crystallinity.<sup>3</sup> The effect of annealing on the skin-core morphology and fracture behavior of hairline-cracked samples was correlated with the toughness and notch sensitivity of virgin polyethylene terephthalate (VPET) and recycled polyethylene terephthalate (RPET) products. The effects of hairline cracks on the notch sensitivity factors for strength ( $k_S$ ) and energy ( $k_T$ ) at the successive crack depths before and after annealing the samples were

determined for comparison to elucidate the effects of hairline cracks and annealing on the fracture behavior of the materials. If cracks have no detrimental effects on the tensile strength and total energy absorbed on deformation, the notch sensitivity factors for strength ( $k_S$ ) and energy ( $k_T$ ) are equal to 1.0. Conversely, if they have detrimental effects, the notch sensitivity factors are greater than 1.0.<sup>1,4</sup> In this study, the effect of hairline cracks and annealing on the fracture modes of the selected materials was evaluated by determining the difference between the notch sensitivity factors of VPET and RPET before and after they were annealed. This helped us to draw conclusions about whether the annealing of PET injection moldings can reduce their sensitivity to hairline cracking.

## MATERIALS AND METHODS

### Material and sample preparation

Amorphous-grade neat PET (VPET) pellets (MA2103 LOT 601K; viscosity average molecular weight=41499 g mol<sup>-1</sup>) were obtained from UNITIKA (Tokyo, Japan), and RPET flakes (viscosity average molecular weight=23131 g mol<sup>-1</sup>) were obtained from Yasuda-Sangyo Group (Kyoto, Japan). VPET pellets were used as received. RPET flakes were extruded and pelletized before injection molding. Flakes were dried at 120 °C for at least 5 h before extrusion by a single-screw extruder (SR-Ruder Bambi SRV-P70/62; Nihon Yuki, Osaka, Japan). The barrel temperature was set between 255 and 290 °C, and the screw rotation speed was 50 r.p.m.

Before injection molding, VPET and RPET pellets were dried for at least 4 h at 130 °C in a PICCOLO hopper-dryer (Itswa, Japan). Dumbbell samples (10×3 mm) were fabricated with a TOYO PSS TI-30F6 injection-molding machine (TOYO, Tokyo, Japan) in a barrel temperature range of 250–270 °C. The mold temperature was set to 30 °C, and the injection and holding pressures were set to 60 kgf cm<sup>-2</sup>.

### Annealing of dumbbell specimens

Specimens were annealed by immersion in hot edible oil. An oil-filled beaker was placed inside an oil-filled electric pot, which was equipped with a temperature-regulating device (thermostat). The oil in the beaker was heated by the electric pot and stirred regularly to maintain a homogeneous temperature. The temperature of the oil in the beaker was regulated at 160 °C and was constantly measured with a thermometer. To avoid twisting of the samples because of melting, each of the samples was held between two flat aluminum bars and dipped in the hot oil for 35 s; time was regulated with a stopwatch. Subsequently, the annealed specimen was cooled in a bath containing 10 °C ice-chilled oil. It is important to note that oil was used in this process because of its non-absorption by the polymer. It is also believed that annealing by direct contact with liquid medium has a more profound effect on the materials than with air medium, which is usually carried out through oven heating.

### Birefringence observation of PET injection moldings

Birefringence was investigated in the cross-section of dumbbell samples to gauge the sizes of the skin and core regions. Before polarized optical microscopy, a short section of the dumbbell specimen was cut and embedded in epoxy. One side of the cross-section was polished with a rotational polishing wheel mounted with abrasives of different grain sizes to achieve smooth surfaces. The abrasives were used in stages from large rough grains to smooth fine grains until a smooth surface was achieved. The surface was further made as smooth and clean as possible by the use of an alumina cleaner. Thereafter, the first polished side was mounted on a clear and clean glass slide with glue to hold it in place and ensure that liquid did not penetrate between the glass and sample surface during the polishing of the opposite end of the specimen. It was then left to dry. The polishing steps described above were repeated for the opposite side of the cross-section until a thin, smooth and translucent view, about 30 μm in thickness, was achieved. Polarized optical micrographs were taken from the polished specimen with a 3.34 megapixel Nikon Coolpix 990 digital camera (Nikon, Tokyo, Japan) attached to a ×10/0.25P magnification optical lens that was mounted on a Nikon ECLIPSE E600 Polarizer (Nikon). The micrographs were joined together using Adobe Photoshop CS software (USA). The resulting composite images (Figures 1 and 2) were converted to grayscale with Origin 7J [Rel v7.0265 (B265)] software (OriginLab, Northampton, MA, USA). Plots of the frequency and amplitude of the gray values were generated for the entire cross-section (10×3 mm).<sup>1</sup>

### Measurement of crystallinity in PET

A JEOL TM-0015 microtome (JEOL, Tokyo, Japan) was used to cut dumbbell specimens into 56 slices along the width direction. Each slice measured 50 μm in thickness. The slices were taken in sequence corresponding to the pseudo-skin, skin, interface and mid-core regions of the specimens. Samples for differential scanning calorimetry were cut from the following slice depths: 50, 550, 1400 and 2500 μm (as indicated in Tables 1 and 2). Differential scanning calorimetry was conducted with a TA Instrument model 2920-modulated differential scanning analyzer (TA Instruments, Tokyo, Japan). Samples were heated from 30 to 300 °C at 10 °C min<sup>-1</sup>. The melting enthalpies ( $E_M$ ) of all specimens normalized with their respective enthalpies of cold crystallization ( $E_C$ ) and melting ( $E_M$ ) were measured from the resulting differential scanning calorimetry curves. The enthalpy of the materials because of processing ( $E_p$ ) was then calculated by the following equation:  $E_p = E_M - E_C$ . The resulting thermal properties of the specimens before and after annealing are shown in Tables 1 and 2, respectively.

### Laser-Raman spectroscopy of the materials

Laser-Raman spectroscopy scanning was conducted along the melt flow direction of the core-deep polished surface of the dumbbell samples. The

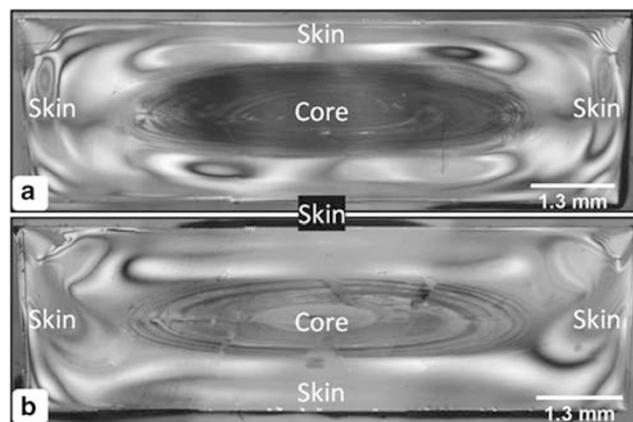


**Figure 1** Birefringence observation of the cross-section dumbbell samples of (a) virgin polyethylene terephthalate and (b) recycled polyethylene terephthalate before annealing, showing their skin-core morphology.

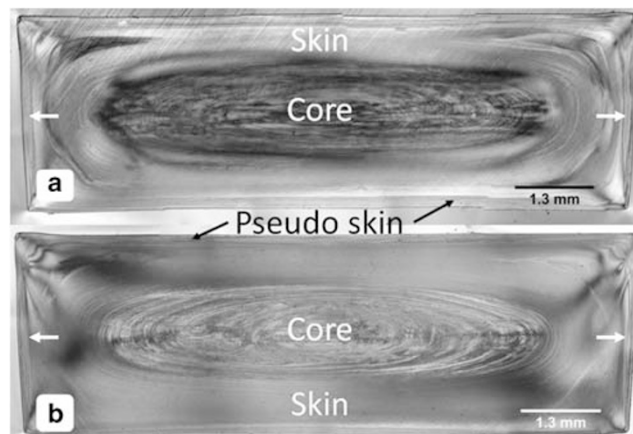


**Figure 2** Birefringence of (a) virgin polyethylene terephthalate and (b) recycled polyethylene terephthalate after annealing, showing the pseudo skin-skin-core morphology (pseudo-skin is indicated by arrows).

Raman spectrum was measured at room temperature with a green laser (532 nm) light source. The diameter of the focused laser beam was 2 μm. All spectra were recorded by 1–3 time integrations after 3-s irradiation to eliminate laser noise. The measuring area was 30×5000 μm with spatial intervals of 10 and 20 μm.

### Cutting of hairline cracks on dumbbell samples

Hairline cracks ranging from 5 to 60 μm in size were introduced on a single edge (thickness) of the dumbbell samples. A SAICAS DN-20S microcutting machine (DAIPLA WINTES, Hyogo, Japan) fixed with a sharp thin cutter blade and mounted with a 100-N load cell was used to perform the notching. The horizontal speed was set at 25 μm s<sup>-1</sup>. The angle of the hairline crack and radius of curvature were measured to be around 8° and 90 μm, respectively, which were much smaller than what is described in ASTM D 256.

### Testing and notch sensitivity characterization

Tensile testing was conducted on the unannealed and annealed dumbbell specimens. An Instron 4466 universal tensile testing machine (Instron, Osaka, Japan) with a 10-kN load cell and cross-head speed set of 10 mm min<sup>-1</sup> was used for performing tensile tests on the specimens. The span length measured 115 mm. At least seven sample pieces were tested for each material and notching condition. The test was conducted at room temperature.

**Table 1 Crystallinity of VPET and RPET injection moldings before annealing**

Materials	Slice depth ( $\mu\text{m}$ )	Cold crystallization ( $E_C$ )		Melting ( $E_M$ )		$E_P=(E_M-E_C)$ Enthalpy ( $\text{Jg}^{-1}$ )
		Enthalpy ( $\text{Jg}^{-1}$ )	Temp. ( $^{\circ}\text{C}$ )	Enthalpy ( $\text{Jg}^{-1}$ )	Temp. ( $^{\circ}\text{C}$ )	
VPET	50	34.1	125.9	69.5	257.4	35.4
	550	20.3	126.0	44.8	256.8	24.5
	1400	22.2	124.6	46.2	256.7	24.0
	2500	10.1	125.2	44.5	256.9	34.4
RPET	50	26.8	130.7	37.3	253.6	10.5
	550	26.1	130.5	37.2	253.7	11.1
	1400	35.0	130.7	49.9	232.9	14.9
	2500	23.1	130.4	39.4	253.4	16.3

Abbreviations: RPET, recycled polyethylene terephthalate; VPET, virgin polyethylene terephthalate.

**Table 2 Crystallinity of VPET and RPET injection moldings after annealing**

Materials	Slice depth ( $\mu\text{m}$ )	Cold crystallization ( $E_C$ )		Melting ( $E_M$ )		$E_P=(E_M-E_C)$ Enthalpy ( $\text{Jg}^{-1}$ )
		Enthalpy ( $\text{Jg}^{-1}$ )	Temp. ( $^{\circ}\text{C}$ )	Enthalpy ( $\text{Jg}^{-1}$ )	Temp. ( $^{\circ}\text{C}$ )	
VPET	50	4.5	123.2	49.1	257.2	44.6
	550	23.1	124.7	48.4	256.9	25.3
	1400	24.2	123.8	52.8	257.4	28.6
	2500	12.7	124.4	54.2	257.4	41.5
RPET	50	27.9	124.4	65.8	254.2	37.9
	550	19.3	128.5	37.7	254.2	18.4
	1400	21.5	129.8	38.6	254.0	17.1
	2500	20.9	129.9	42.4	253.6	21.5

Abbreviations: RPET, recycled polyethylene terephthalate; VPET, virgin polyethylene terephthalate.

### Determination of notch sensitivity factors

Investigations were conducted on the effects of hairline cracks by analyzing the notch sensitivity factors for strength ( $k_S$ ) and energy ( $k_T$ ) at different crack depths for VPET and RPET samples before and after they were annealed. This gives an understanding of the effects of hairline cracks and annealing on the fracture behavior of the materials. If cracks have no detrimental effects on the tensile strength and total energy absorbed on deformation, the notch sensitivity factors for strength ( $k_S$ ) and energy ( $k_T$ ) are equal to 1.0. Conversely, if they have detrimental effects, the notch sensitivity factors are greater than 1.0.<sup>1,4</sup> Therefore, the effect of annealing on the toughness of the materials is determined by the difference between the notch sensitivity factors for unannealed and annealed samples. In this study, notch sensitivity factors were determined by the following equations:<sup>1,4</sup>

$$k_S = \left[ \frac{(YS_0) \times [t(w - a_i)]}{(YS_i) \times (tw)} \right] \quad (1)$$

$$k_T = \left[ \frac{A_{0ssc} \times [t(w - a_i)]}{A_{issc} \times [tw]} \right] \quad (2)$$

where  $k_S$  is the notch sensitivity factor for yield strength and  $k_T$  is the notch sensitivity factor for energy.  $YS_0$  and  $YS_i$  are the yield stress (strength) of unnotched and notched samples, respectively (subscript  $i$  is the successive

notch depths),  $t$  is thickness,  $w$  is width and  $a$  is notch depth.  $A_{0ssc}$  and  $A_{issc}$  are the areas under the stress–strain curves for unnotched and notched specimens, respectively.<sup>1,4</sup>

The notch sensitivity factor for yield/fracture strength gives an understanding of how hairline cracks affect the strength of materials. On the other hand, the notch sensitivity factor for energy measures the effect of hairline cracks on the toughness of the materials.

## RESULTS AND DISCUSSION

### Morphology characterization of the birefringence observation of the samples

Figures 1a and b show the birefringence of the cross-sections of VPET and RPET samples before they were annealed.<sup>1</sup> The figure reveals distinct skin-core regions that enclose an interfacial region. Figures 2a and b show their birefringence after they were annealed. The images clearly reveal the creation of an outer skin, referred to as a pseudo-skin (indicated by the arrows). Hence, after the materials were annealed, three distinct regions, namely, the pseudo-skin, skin and core regions, could be seen. The conversion of images to grayscale and the generation of subsequent plots defining the intensity of the gray areas were performed using Origin 7).<sup>1</sup> The resulting plots for the unannealed samples are depicted in Figures 3a and b.<sup>1</sup> The images reveal a complex morphology, which clearly shows the existence of the skin, interface and core regions in the samples. Conversely, the plots for the annealed samples are shown in Figures 4a and b. This figure depicts the introduction of the pseudo-skin resulting from annealing and also shows the skin, interface and core regions.

Derivations from the intensity of the gray areas were used to determine precisely the thickness of the pseudo-skin, skin, interface and core regions, as shown in Figures 3 and 4. The plots marked with W and X represent the intensity values of the grayscale in the width and thickness directions of the samples, respectively.<sup>1</sup> The horizontal and vertical cursors on the matrix were adjusted along the width and thickness directions until well-defined frequency peaks were obtained at each region. The center region between the two maximum peak intensities obtained from W and X plots in each region was taken to be the pseudo-skin, skin, interface or core width and thickness.<sup>1</sup>

The contour plots of the matrices before and after annealing are shown in Figures 5 and 6, respectively. The contours of the unannealed samples in Figure 5a show that VPET had well-defined skin-core morphology with the presence of an interface between the two regions. Figure 6a indicates that VPET still had well-defined morphology. However, the contours are more dispersed and relaxed, and the intensity is not as strong as it was in the unannealed samples, suggesting slight morphological changes<sup>1,5</sup> in the bulk of the material. Figure 5b shows that, before annealing, the contours of RPET also had distinct skin-core morphology, but these are more dispersed and not as strong and intense as what was seen in VPET. However, after the material was annealed, the contours of RPET became more dispersed and relaxed without any defined boundaries, suggesting phenomenal morphological changes in the material.<sup>1,5</sup> The difference in morphology before and after the annealing of VPET is clearly seen in the Raman spectra in Figure 7 (plots 1 and 2, respectively). The introduction of pseudo-skin after the annealing of VPET could be clearly seen at the point marked X on plot 2, which measures  $\leq 400 \mu\text{m}$ . On the other hand, RPET showed a more homogeneous skin-core structure in the unannealed and annealed specimens, as shown in Figure 8 (plots 1 and 2, respectively).

The distinct boundaries and high intensity of the contours before annealing could have resulted from high-molecular orientation, especially at the skin layer, during injection molding. The slow crystallizing

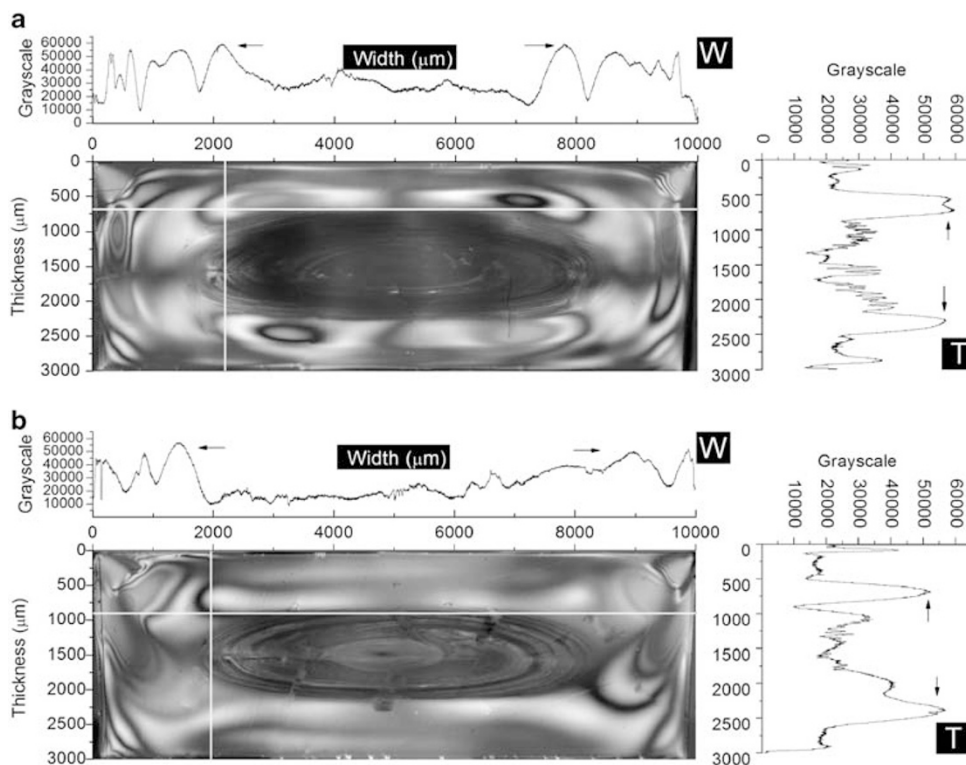


**Figure 3** Gray-image plots of (a) virgin polyethylene terephthalate and (b) recycled polyethylene terephthalate before annealing, showing the gray values of the skin, interface and core regions (W: graph of gray values in the width direction; X: graph of gray values in the thickness direction).

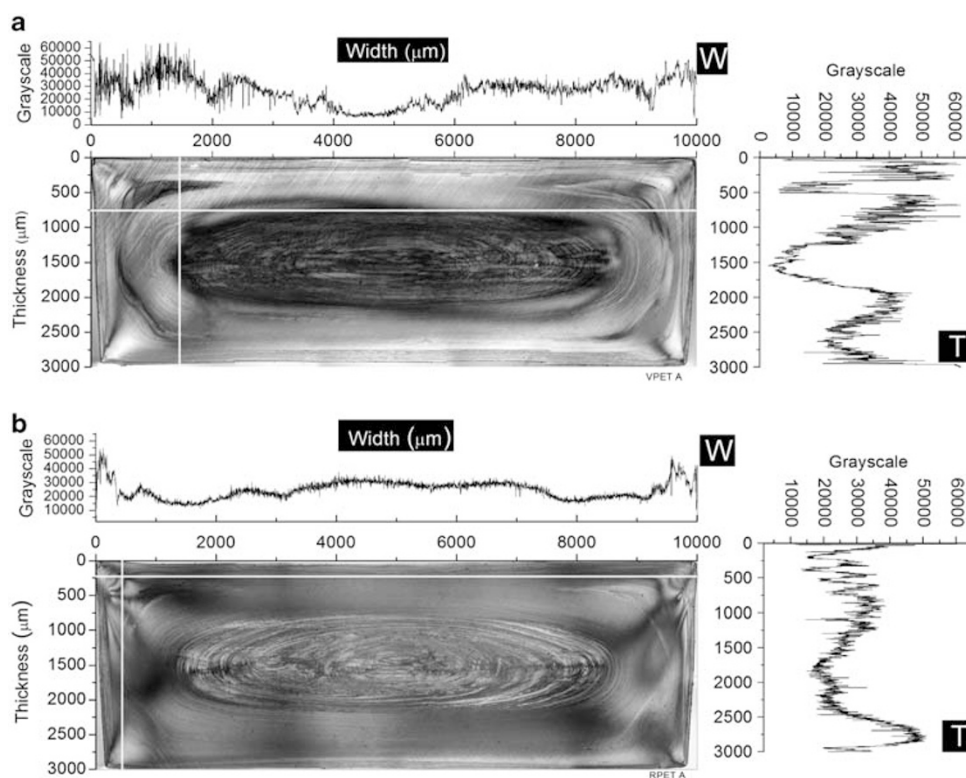


**Figure 4** Gray-image plots of (a) virgin polyethylene terephthalate and (b) recycled polyethylene terephthalate after annealing, showing the gray values of the pseudo-skin, skin, interface and core regions (W: graph of gray values in the width direction; X: graph of gray values in the thickness direction).

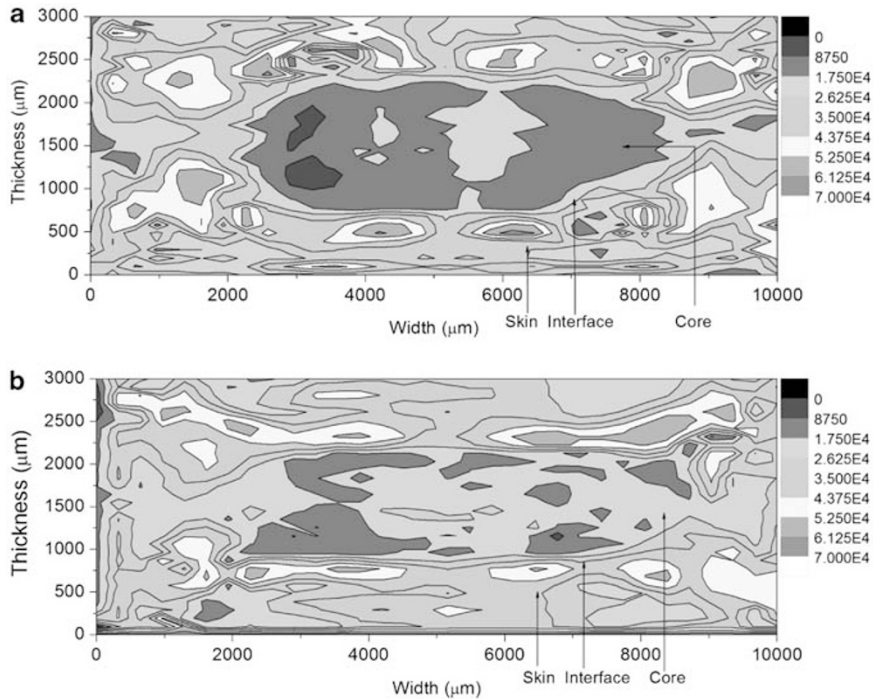


**Figure 5** Image contour plots of (a) virgin polyethylene terephthalate (VPET) and (b) recycled polyethylene terephthalate (RPET) before annealing, showing the skin, interface and core regions (W: graph of gray values in the width direction; X: graph of gray values in the thickness direction).

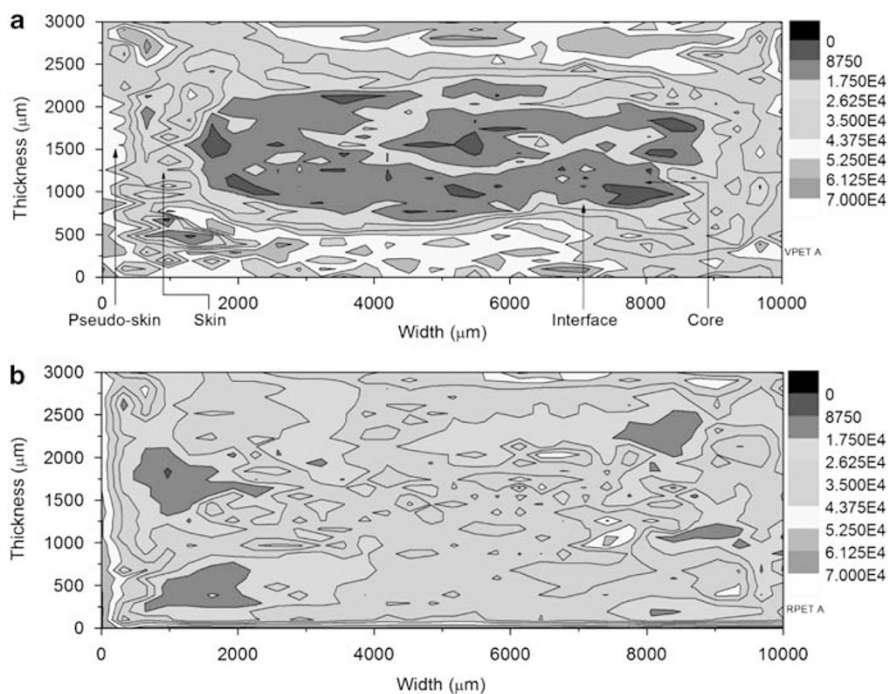


**Figure 6** Image contour plots of (a) virgin polyethylene terephthalate (VPET) and (b) recycled polyethylene terephthalate (RPET) after annealing, showing the pseudo-skin, skin, interface and core regions (note: RPET has no identifiable boundaries between the regions).

nature of PET resulted in well-formed crystals at the core region, which accounts for the strong intensity of the contours in the region. The intensity of the contours between VPET and RPET is believed to depend on the length of the molecular chains, as well as on the size of

the crystals. Whereas VPET is known to have large crystals, RPET has small crystals. In Figures 6a and b, the dispersed and relaxed nature of the contours and the absence of a clear skin-core boundary, especially in RPET, suggest morphological changes,<sup>1,5</sup> which was a direct effect

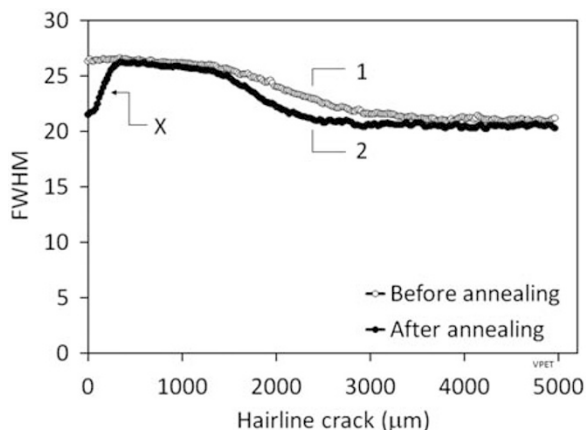


**Figure 7** Full-width at half-maximum (FWHM) of Raman intensity of virgin polyethylene terephthalate (VPET) before and after annealing.

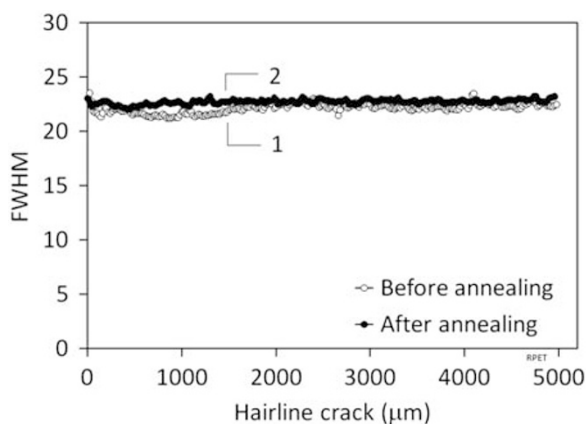


**Figure 8** Full-width at half-maximum (FWHM) of Raman intensity of recycled polyethylene terephthalate (RPET) before and after annealing.

of annealing. The materials were annealed at 160 °C, above the glass transition temperatures ( $T_g$ ) of the materials. At this temperature, materials are already in the rubbery phase. Subsequent quenching of the materials in  $\leq 10^\circ\text{C}$  ice-chilled oil disrupted the slow crystallization process, which could have resulted in the formation of more developed crystals in the core regions of the samples. Consequently, the contour appeared more relaxed and dispersed in the materials (Figures 6a and b).

#### Evaluation of the crystallinity of VPET and RPET before and after annealing using differential scanning calorimetry and Raman spectroscopy

Table 1 shows the thermal properties of unannealed VPET and RPET materials. The enthalpies and temperatures resulting from cold crystallization and melting, as recorded from differential scanning calorimetry, were measured from the following slice depths: 50, 550, 1400 and 2500  $\mu\text{m}$ . The enthalpy due to processing ( $E_p$ ) indicates that VPET has a high enthalpy at the 50- $\mu\text{m}$  depth of the skin layer. This could be the effect of transitional changes of the resin from the fluid state to the rubbery and, ultimately, the crystallized state.<sup>2,6</sup> Chain orientation and crystal size could be other factors that increase the crystallinity of the topmost skin layer. The value of the enthalpy, however, decreased at a slice depth of 550–1400  $\mu\text{m}$ . However, there is

a remarkable increase in the enthalpy at a depth of 2500  $\mu\text{m}$ , which is the core region of the samples. Because of the slow crystallization process of semicrystalline PET, the crystals in the core region had enough time to develop, resulting in higher crystallinity.<sup>2,6</sup>

The unannealed samples of RPET showed enthalpies that are more similar at the different slice depths of the skin (50–550  $\mu\text{m}$ ). Table 1 indicates that the enthalpies for RPET are about 50% less than the enthalpies of VPET, which signifies lower crystallinity. A similar level of crystallinity at the skin region could arise from the small sizes of the crystals in RPET, which do not change remarkably during thermal transition from the liquid to the crystallized state.<sup>2</sup> Nevertheless, there was an appreciable increase in the enthalpy when the slice depths penetrated 1400–2500  $\mu\text{m}$ , as shown in Table 1, where the interface and core regions of the dumbbell samples are located. It could be concluded from Table 1 that the unannealed VPET is more crystallized at different slice depths than is RPET.

Table 2 shows remarkable changes in the values of the enthalpies after the samples were annealed. It is evident from Table 2 that VPET had a phenomenal change in enthalpies because of processing at the 50- $\mu\text{m}$  slice depth. This signifies the introduction of a more crystallized pseudo-skin, which is a direct effect of annealing the materials. Annealing did not appear to have significant effects on the enthalpies of VPET at a slice depth of 550–1400  $\mu\text{m}$ . This could be due to the effect of quenching the materials in  $\leq 10^\circ\text{C}$  ice-chilled oil on their heat conduction within the intermediate skin regions. However, there was a significant increase in the enthalpy when the slice depth penetrated 2500  $\mu\text{m}$ , the core region depth. After annealing, Table 2 shows that, although the enthalpies due to cold crystallization in VPET increased slightly at the 550–250- $\mu\text{m}$  depth, the same values decreased in RPET. However, Table 2 reveals that the enthalpy due to processing is higher in VPET than in RPET.

Figures 7 and 8 depict the full-width at half-maximum spectral intensity of the unannealed and annealed samples of VPET and RPET, respectively. Plot 1 of Figure 7 indicates that the crystallinity of unannealed VPET increased gradually within the skin region, which measures about 1500  $\mu\text{m}$ . However, there is an outstanding increase in the crystallinity of VPET when the slice depth penetrated the interfacial region ( $\geq 1500 \mu\text{m}$ ). The crystallinity continued to increase at the core depth ( $\geq 1700 \mu\text{m}$ ). Point X on plot 2 (Figure 7), on the other hand, shows that a significantly crystallized pseudo-skin, measuring about 400  $\mu\text{m}$ , was created in VPET when it was annealed. The crystallinity of VPET at the natural skin did not seem to change remarkably, after it was annealed. However, there was a considerable increase in crystallinity at the interfacial layers, whereas the core region had a mild increase in crystallinity. These observations are corroborated by the differential scanning calorimetry results shown in Tables 1 and 2.

Figure 8 (plots 1 and 2) shows that there was more homogeneous skin-core morphology in RPET before and after it was annealed. However, plot 2 shows that when RPET was annealed, the non-distinct skin-core boundary that was seen in the unannealed samples virtually disappeared. This suggests that annealing RPET above  $T_g$  and quenching it in  $\leq 10^\circ\text{C}$  ice-chilled oil could have reduced the sizes of its crystal along the entire bulk of the material. The full-width at half-maximum intensity values appear to be consistent with the results of the differential scanning calorimetry shown in Tables 1 and 2.

#### Effect of hairline cracks and annealing on the mechanical properties of VPET and RPET

Figures 9a and b show the typical stress–strain curves of VPET and RPET before annealing, depicting their fracture behaviors at different hairline crack depths. The corresponding typical stress–strain curves

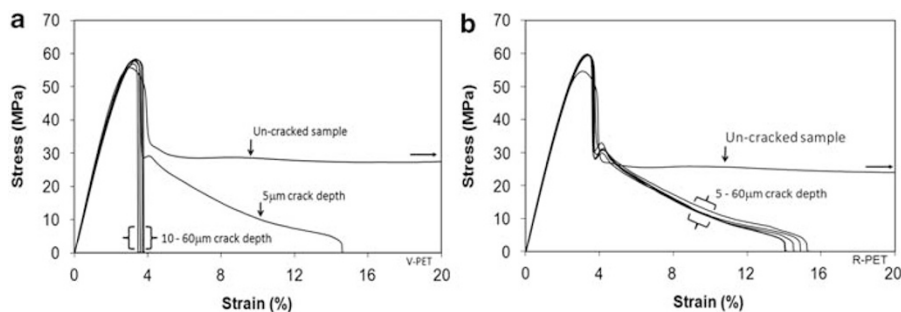


**Figure 9** Stress–strain curves of (a) virgin polyethylene terephthalate (VPET) and (b) recycled polyethylene terephthalate (RPET), showing fracture behaviors before annealing.

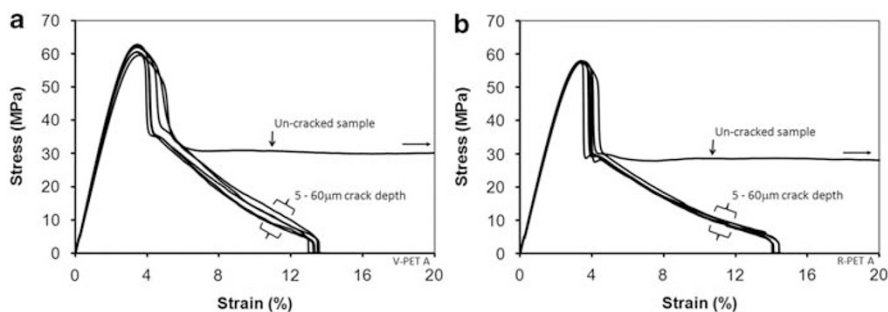


**Figure 10** Stress–strain curves of (a) virgin polyethylene terephthalate (VPET) and (b) recycled polyethylene terephthalate (RPET), showing fracture behaviors after annealing.

for annealed specimens are shown in Figures 10a and b for VPET and RPET. The mechanical properties are shown in Table 3. Table 3 shows that before annealing, VPET and RPET had yield stresses between 55 and 58 MPa (Figures 9a and b) when they were unnotched and when 5–60  $\mu\text{m}$ -deep hairline cracks were introduced. However, when samples were annealed, VPET had a remarkable increase in yield stress, as shown in Figure 10a, for the same (5–60  $\mu\text{m}$ ) hairline crack depths. On the other hand, the yield stress of RPET decreased slightly (see Figure 10b) at different hairline crack depths. This could be the effect of more homogeneous bulk material resulting from annealing, as recorded in the enthalpies in Table 2. This is equally seen in the Raman full-width at half-maximum intensity shown in Figure 8. It should be noted that the slight decrease in the yield stress of RPET could have resulted from a reduction in the size of the crystals after annealing and subsequent quenching. Annealing is also believed to remove internal stresses from the materials, thereby increasing the materials' toughness. It is equally evident that notched samples exhibited higher yield stresses than did unnotched samples. This could be the effect of the notch, which changes the biaxial stress to a triaxial stress field<sup>1,4,7</sup> and increases the materials' resistance to fracture. Studies show that the strain rate at the crack tip is greater than the strain rate at any other region on the test piece. Therefore, notches or cracks change the nature of the stress field from a uniaxial tensile stress to a triaxial stress in the region of the crack. This brings about bending (twisting) of the test sample, resulting in a tearing fracture.<sup>1,4,7</sup> Results suggest that the yield stress of the materials is not sensitive to the range of hairline cracks under study.

Table 3 shows that, before the materials were annealed, the unnotched samples did not fracture below 300% strain.<sup>1</sup> However, the introduction of a mere 5- $\mu\text{m}$  deep hairline crack in the materials resulted in a drastic change in the fracture behavior of VPET and

**Table 3** Mechanical properties of VPET and RPET samples before and after annealing

Materials	Hairline crack depth ( $\mu\text{m}$ )	Before annealing		After annealing	
		Yield stress	% Strain	Yield stress	% Strain
VPET	Unnotched	55.2	>300	59.9	<100
	5	57.6	14.8	61.7	13.2
	10	58.0	4.2	61.7	13.3
	20	58.1	3.8	61.6	13.3
	40	58.3	3.7	62.8	13.4
RPET	60	57.9	3.5	61.1	13.1
	Unnotched	54.19	>300	57.6	>300
	5	59.1	15.3	57.7	14.1
	10	59.3	14.7	57.7	14.1
	20	59.3	15.1	57.5	14.2
	40	60.0	14.0	57.8	14.2
	60	58.7	14.7	57.8	14.3

Abbreviations: RPET, recycled polyethylene terephthalate; VPET, virgin polyethylene terephthalate.

RPET, in which the strain decreased from about 300% to 14–15.5%, as shown in Figures 9a and b. This marked a transition from ductile to semiductile fracture behavior. Further deepening of the crack to 10  $\mu\text{m}$  resulted in a brittle failure (4.2–3.5% strain) in VPET (Figure 9a), which could be attributed to higher crystallinity,<sup>1</sup> as shown by the enthalpies in Table 1. This is also evident in the full-width at half-maximum values of the Raman spectra in plot 1, Figure 8. Conversely, the unannealed RPET continued to fracture in a semiductile manner, even at a hairline crack depth of 60  $\mu\text{m}$ , as shown in Figure 9b.

The results reveal that, in contrast to the unannealed VPET specimens, the annealed samples experienced a semiductile fracture at all crack depths (Figures 10a and b). This could be the direct effect of annealing and quenching of the samples, which could result in the relaxation of internal stress in the material. RPET, on the other hand, continued to fracture in a semiductile manner after it was annealed, and seems to show no significant change in its strain percentage. It could be concluded that annealing the samples, particularly VPET, created a protective pseudo-skin that not only increased the yield stress but also minimized the triaxial effect<sup>7</sup> of hairline cracks on the natural skin. The removal of internal stress could be another effect of annealing, which resulted in improved ductility in the materials, especially VPET.

#### Hairline crack sensitivity of VPET and RPET before and after annealing

Figures 11 and 12 show the notch sensitivity factors for strength ( $k_S$ ) for VPET and RPET, respectively, as calculated by Equation 1. It can be seen from Figure 11 that, before annealing,  $k_S$  values for VPET were between 0.95 and 1.0. However, after annealing,  $k_S$  increased slightly to between 0.97 and 1.0. Figure 12 shows that  $k_S$  values for RPET were between 0.9 and 1.0 when the material was not annealed, and after annealing, there was a remarkable increase in the values of  $k_S$  (1.0) for RPET. The value  $k_S$  is known to be equal to 1.0 if notches have no

detrimental effects on the yield stress of the materials, otherwise it is greater than 1.0.<sup>1,4</sup> These results suggest that annealing led to a reduction in the triaxial stress effect of the notches<sup>7</sup> on the materials resulting from the creation of the pseudo-skin and removal of internal stresses. Figure 9 shows that the values of  $k_S$  (0.95–1.0) in VPET at different hairline crack depths are slightly higher than those in RPET (0.9–1.0) before annealing, as shown in Figure 12. This suggests that, although the values are still close to 1.0, the yield stress of RPET is more affected by hairline cracks than that of VPET because of lower crystallinity [refer to Table 1], resulting in higher triaxial stress effects.<sup>7</sup> However, after annealing, the values of  $k_S$  for RPET increased remarkably and became higher than those for VPET, which signifies a reduction in the notch sensitivity of RPET. This could be attributed to the presence of the more crystallized pseudo-skin and relaxation of internal stresses. The pseudo-skin could have increased the modulus of resilience at the edges and minimized the triaxial stress effect of hairline cracks,<sup>7</sup> which would have occurred at the natural skin because of its highly amorphous structure. It can be concluded that the increase in yield stress recorded for VPET after annealing was principally due to the increase in the modulus of resilience provided by the pseudo-skin. It could also be concluded that the triaxial stress resulting from the notches,<sup>7</sup> which would have increased the yield stress, was minimized. It is important to observe that all the hairline cracks ( $\leq 60\ \mu\text{m}$ ) were within the pseudo-skin region ( $\approx 400\ \mu\text{m}$ ).

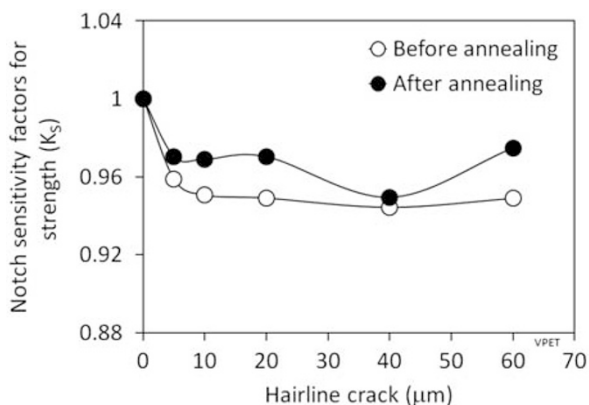


**Figure 11** Notch sensitivity factors for strength ( $k_S$ ) of virgin polyethylene terephthalate (VPET) before and after annealing.

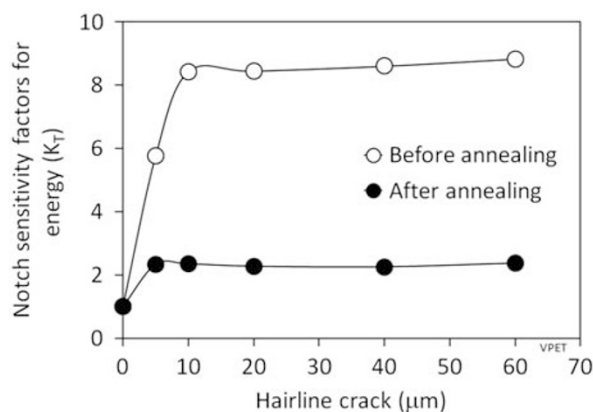


**Figure 13** Notch sensitivity factors for energy ( $k_T$ ) of virgin polyethylene terephthalate (VPET) before and after annealing.

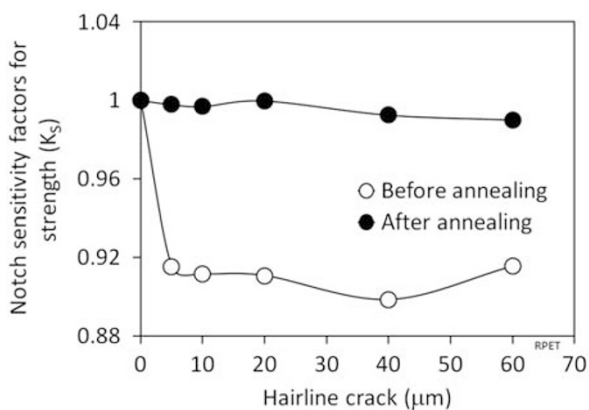


**Figure 12** Notch sensitivity factors for strength ( $k_S$ ) of recycled polyethylene terephthalate (RPET) before and after annealing.

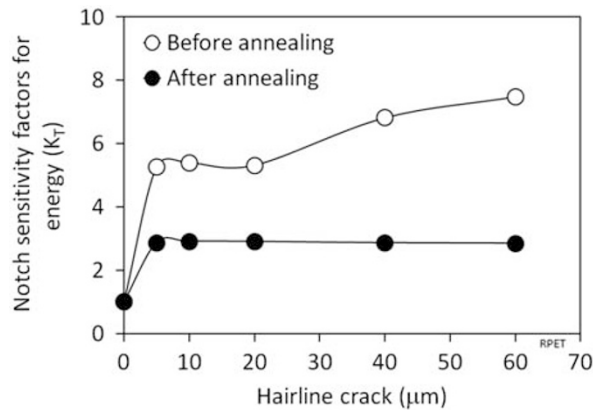


**Figure 14** Notch sensitivity factors for energy ( $k_T$ ) of recycled polyethylene terephthalate (RPET) before and after annealing.



Figure 12 reveals that the values of  $k_S$  for RPET before annealing were lower than those of VPET. This resulted from the lower crystallinity in the amorphous skin of RPET. The small sizes of the crystals in RPET and the loose nature of the molecular chains in the skin region encourage easy plastic flow and a triaxial stress effect when notches are present.<sup>7</sup> Therefore, the gain in yield stress in the notched samples could be mainly due to triaxial stress effects.<sup>7</sup> Previously, results showed that, after annealing, the skin-core morphology of RPET was dispersed and its boundaries became non-existent (Figures 6b and 8). This means that the entire bulk is homogeneous in structure. The dispersion in the bulk of RPET is reflected in the values of  $k_S$  for RPET shown in Figure 12. It is clear that the values of  $k_S$  are approximately equal to 1.0 at all of the crack depths, which were still within the pseudo-skin region. It can be concluded that there was more homogenous and relaxed bulk material in RPET than in VPET after annealing and quenching, which resulted in equal values of yield stress and  $k_S$  in RPET at different hairline cracks.

The notch sensitivity factors for energy ( $k_T$ ) are calculated from Equation 2 and shown in Figures 13 and 14. The values of  $k_T > 5.0$  in Figure 13 show that a mere 5- $\mu\text{m}$ -deep hairline crack had a detrimental effect on the toughness of VPET before it was annealed. This means that the material was sensitive to the hairline crack and experienced a drastic change from highly ductile to semiductile fracture behavior. When the hairline crack was deepened to  $\geq 10 \mu\text{m}$ , VPET fractured in a brittle manner, and  $k_T$  increased to more than 8.0 and remained constant. However, when VPET was annealed, the values of  $k_T$  decreased to about 2.0, signifying substantial reduction in the notch sensitivity of VPET. However, before annealing, the values of  $k_T$  for RPET remained  $< 6.0$ , as the material continued to fracture in a semiductile manner, with notches  $\leq 20 \mu\text{m}$  deep. These values slightly increased above 6.0 but were  $< 8.0$ , which is still a semiductile fracture range. The values of  $k_T$  show that, before annealing, VPET is more sensitive to hairline cracks and fractures in a brittle manner compared with RPET when the crack is  $\geq 10 \mu\text{m}$  deep. The major reason for the high notch sensitivity in VPET is the higher level of crystallinity (Table 1 and Figure 7).

It can be seen from Figures 13 and 14 that there was remarkable decrease in the notch sensitivity factors for energy ( $k_T$ ) in VPET and

RPET, respectively. It is obvious that annealing significantly improved the toughness of VPET, which resulted in a decrease in the preannealing value of  $k_T$  from between 5.0 and 9.0 to  $< 3.0$ . It is also remarkable to note that VPET fractured in a similar semiductile manner as RPET. The results also reveal that, after annealing, hairline cracks affected the toughness of VPET in a manner similar to the toughness of RPET. RPET also showed a remarkable reduction in sensitivity to all hairline crack depths.

## CONCLUSION

This study has shown that the annealed VPET and RPET experienced semiductile fracture behavior under tensile loading at notch depths of 5–60  $\mu\text{m}$ . This semiductile transition suggests that annealing is effective in reducing brittle fracture in PET. The results show that annealing creates a more crystallized pseudo-skin, which measures about 400  $\mu\text{m}$  in the materials. The pseudo-skin has proved to provide a higher modulus of resilience and minimizes the triaxial effect of stress (because of cracks) in the materials, which would have occurred on a more amorphous and less-crystallized skin region. Therefore, it can be concluded that annealing in 160 °C hot edible oil and quenching in  $< 10$  °C ice-chilled oil is a good approach to reduce hairline crack sensitivity in PET injection moldings.

- 1 Ogazi-Onyemaechi, B. C., Leong, Y. W. & Hamada, H. Crack propagation behavior and toughness of V-Notched polyethylene terephthalate injection moldings. *J. App. Pol. Sc.* **116**, 132–141 (2010).
- 2 Sancaktar, E., Negandhi, N. & Adwani, S. Evaluation of processing effects in injection-molded amorphous and crystalline thermoplastics using an Excimer Laser. *J. App. Pol. Sc.* **101**, 258–268 (2006).
- 3 Chapleau, N. & Huneault, M. A. Impact modification of poly(ethylene terephthalate). *J. App. Pol. Sc.* **90**, 2919 (2003).
- 4 Takano, M. & Nielsen, L. E. The notch sensitivity of polymeric materials. *J. App. Pol. Sc.* **20**, 2193–2207 (1976).
- 5 Zhao, J., Yang, J., Song, R., Linghu, X. & Fan, Q. The effect of annealing on the subsequent cold crystallization of amorphous poly(ethylene terephthalate). *Euro. Pol. J.* **38**, 645–648 (2002).
- 6 Fernandez, M. R., Merino, J. C. & Pastor, J. M. Micro-Raman spectroscopy investigations of the skin-core morphology. *Pol. Eng. Sc.* **40**, 95–107 (2000).
- 7 Arends, C. B. (ed.). *Polymer Toughening* 61–83 (Marcel and Dekker, New York, 1996).